Fatigue behaviour of PBF additive manufactured TI6AL4V alloy after shot and laser peening

Santiago Aguado-Montero [a], Carlos Navarro [a,*], Jesús Vázquez [a], Fernando Lasagni [b], Sebastian Slawik [c], Jaime Domínguez [a,d]

[a] *Department of Mechanical Engineering and Manufacturing, Universidad de Sevilla, Spain*
[b] *Advanced Center for Aerospace Technologies (CATEC), 41903 La Rinconada, Seville, Spain*
[c] *Department of Materials Science and Engineering, Saarland University, 66123 Saarbrücken, Germany*
[d] *Laboratory of Engineering for Energy and Environmental Sustainability, Universidad de Sevilla, 41092 Seville, Spain*

ARTICLE INFO

ABSTRACT

Additive manufacturing (AM) of metallic parts is a relatively new manufacturing procedure. Many industry sectors, such as the aerospace or automotive sectors, have started to apply this technology to produce some elements, thus reducing costs and weight. Several metallic alloys have been employed for AM. Due to the high strength-to-density ratio, Ti6Al4V alloy is probably the alloy most used for AM in the aerospace industry. This alloy usually shows good static strength properties. However, the presence of internal defects and the surface roughness result in a fatigue strength that is clearly lower than that of materials produced by traditional processes. Moreover, the scatter of the fatigue results is generally higher than in the case of wrought pieces.

Different treatments have been proposed to improve the fatigue behavior by reducing internal defects and roughness or generating a favorable residual stress field. In this work, selected surface treatments were considered to improve the fatigue strength of AM parts, including shot and laser peening as well as a combination of shot peening plus chemical assisted surface enhancement (CASE®). Three groups of specimens, each with one of the surface treatments, were fatigue tested to compare the results produced by these treatments. The residual stresses, roughness and hardness produced by the treatments were analyzed. After testing, the fracture surfaces were also analyzed to better understand the fatigue process of the different groups of specimens. The results indicate that laser peening produced the best results, followed by shot peening plus CASE and shot peening. In all three cases, the fatigue strength was much higher than that of the reference group without surface treatment. It was also observed that all failures initiated from an interior defect in the shot peening plus CASE group, four out of six failures in the laser peened group, but only one failure in the case of shot peened group and none in the reference group. Failures of specimens with initiation from internal defects started from defects located deeper than the compressive residual stress layer produced by the treatments.

1. Introduction

The recent development of additive manufacturing (AM) technology for production metal parts has been very rapid [1]. Different metal alloys have been used for AM of structural parts, such as aluminum or titanium alloys, nickel-based alloys or stainless steels. For titanium alloys, the use of Ti6Al4V alloys has been extended for structural purposes, especially for aerospace applications. The relatively low density and good monotonic mechanical properties make AM Ti6Al4V pieces excellent for use in some structural parts of satellites and launchers. However, when the loads applied to the pieces are susceptible to produce fatigue, the Ti alloy components, and also any metallic component produced by AM, encounter problems of strength and reliability [2,3]. These materials present a lower strength than their counterparts produced by any of the traditional methods, such as cast or wrought material, and the variability of the results from one specimen to another under the same loads is usually much higher [4–6]. This circumstance prevents the application of AM structural elements in the aeronautical

---

industry, where reliability is one of the main concerns. The AM process, with very high local temperatures required to melt the powder travelling along the specimen surface and fast cooling, produces internal pores, anisotropy in the microstructure and residual stresses that are very difficult to control and estimate [7–12]. Additionally, the roughness of the pieces produced by this procedure is usually high and has a different pattern than that produced by machining [13,14]. All these specific characteristics of the AM pieces produce an effect on fatigue that is difficult to assess and make its study very important to improving the fatigue strength and reliability of these pieces.

Powder bed fusion (PBF) is one of the most extensive methods for AM of metals, and among them, selective laser melting (SLM) is widely used for Ti6Al4V. As mentioned above, the fatigue strength of AM specimens is usually lower than the strength of their counterparts manufactured by traditional procedures because of certain special microstructural and mechanical features produced by the AM process. Some of these special characteristics are surface roughness, porosity, anisotropy or residual stresses, which, in addition to reducing the fatigue strength, increase the scatter of fatigue lives in tests performed under the same cyclic loads. Many different solutions have been proposed to reduce these detrimental characteristics and to improve the fatigue strength, some relative to the manufacturing process and other to postprocessing treatments. In the first group, solutions are oriented to select the optimum manufacturing parameters, such as platform temperature, laser power, forward speed, manufacturing path or the specimen's relative orientation to the platform, all of which reduce surface roughness, defects or residual stresses [15–20]. In the second group, treatments range from mechanical to thermal or thermomechanical treatments, such as machining, annealing, hot isostatic pressing (HIP) and shot and laser peening. Thermal and thermomechanical treatments usually affect the complete element. Thermal treatments are commonly applied only to eliminate residual stresses or also to modify the microstructure, thus reducing anisotropy and residual stresses [21–24]. The best-known thermomechanical treatment for AM components is HIP, which is applied to eliminate or reduce the number and size of internal defects, thus modifying also the microstructure and eliminating residual stresses [21,24–28].

Surface treatments are oriented mainly to reducing surface roughness and defects close to the surface, generating compressive residual stresses or a combination of these. Milling, turning, grinding or machine polishing produce a clear reduction in roughness and consequently a significant increase in fatigue strength [10,22,29–33]. However, the porosity of the AM components usually makes the strength increment smaller than expected according to the improvement of the surface roughness produced by the above processes. The existence of pores or lack of fusion defects makes crack initiation move from the surface to the interior, where these defects act as stress raisers. This problem can be solved, at least partially, by HIP. HIP reduces the size and number of pores, and when applied in addition to surface polishing, it produces fatigue strength close to that obtained by manufacturing the component via traditional methods, such as wrought or cast materials [4,18,21,25,27]. Other surface treatments used to reduce roughness are chemical polishing, electropolishing or mass finishing, such as barrel tumbling, vibrating polishing or centrifugal polishing [25,34–38]. These methods do not produce such a high reduction of roughness, as with mechanical polishing, but offer some other advantages as allowing mass production or treating surfaces not accessible by machining. These treatments also produce limited fatigue strength increments and thus require the elimination or reduction of internal defects to obtain a higher strength increase. In AM, sand blasting (SB) is an almost standard practice used to reduce the surface roughness [22,26], mainly by eliminating the adhered and partially melted powder particles and, especially in low yield limit alloys such as Al alloys, by producing plastic strain close to the surface and small compressive residual stresses [23]. In recent years, laser polishing has also been proposed as a surface treatment to reduce roughness, which also eliminates pores and defects

close to the surface [39–42]. As a drawback, this treatment generates traction residual stresses close to the surface, negatively affecting the fatigue behavior, but a further stress relief treatment can eliminate them and thus increases the strength [42]. In general, it can be said that reducing the surface roughness produces an increase in fatigue strength [6,22] and that for Ti6Al4V, the combination of fine surface polishing and HIP allows the fatigue strength to approach that obtained by manufacturing the component by traditional methods, such as wrought or cast materials [4,18,21,22,25–27,31,39].

Other groups of surface treatments are those that produce compressive residual stresses close to the surface, a modification of the surface finish, and in many cases, a reduction in the number or size of defects close to the surface. Centrifugal polishing, ultrasonic impact treatment, ball burnishing and ultrasonic shot peening are some of these methods [23,38,39,43,44]. Shot peening (SP) is widely used as a palliative against fatigue [45–47] and has been applied to different metal alloys, such as Inconel 718 [38], 316L stainless steel [48], AlSi10Mg [49–51], Ti-2.5Cu [24] or Ti6Al4V [25,39,52,53]. In all cases of treated specimens where roughness, hardness, porosity or residual stresses were measured, SP produces a small reduction in roughness, as well as an increase in hardness, a reduction in porosity and a nice amount of compressive residual stresses close to the surface. For SP applied to SLM AM Ti6Al4V alloy, in all cases, it produced an increase in fatigue strength relative to the material conditions immediately before applying the surface treatment. Benedetti et al. [25] found no increase in the fatigue limit relative to the original tribofinished specimens but noted an approximately 25% strength increment for intermediate lives. Kahlin et al. [39] found a strength increment of approximately 70% relative to the original as-built specimens. Wycisk et al. [51] obtained an increment of 100% relative to the as-built surface finish but a reduction of 15% relative to the polished specimens, and Navarro et al. [53] showed an increase in strength between 35% and 70% for fatigue lives between 10^4 and $5 \cdot 10^6$ cycles. Laser peening (LP) [24,39,48,53,54] has also been proposed as a surface treatment for AM pieces to improve their fatigue strength, mainly because it usually generates high compressive residual stresses, which are generally lower than those produced by SP but extend along a deeper zone from the surface [24,39,53]. A reduction in porosity close to the surface of the specimen in AM AlSi10Mg treated with LP has also been reported [54]. Regarding the fatigue strength of LP specimens compared to SP specimens, there are some contradictory results. Kahlin et al. [39] obtained a fatigue strength that was approximately 25% lower with AM Ti6Al4V than with SP. Navarro et al. [53] obtained an approximately 25% higher strength for the same material than for SP pieces, and Hackel et al. [48] found a 20% increase in fatigue strength in notched AM 316L steel specimens relative to SP pieces. In any case, there is a very limited set of experimental fatigue data in the literature on the effect of LP treatments of AM pieces. However, the benefits produced by LP when applied to components manufactured by traditional procedures [55] make this surface treatment promising for AM pieces. Among the treatments that produce compressive residual stresses, shot peening is the most accepted; although with contradictory results regarding fatigue strength improvement; it is mainly produced by the detrimental effect of surface roughness and defects close to the surface, which jeopardize the beneficial effect of compressive residual stresses. Similar effects are produced in laser peened specimens. Considering the detrimental effects of roughness and defects, all of these treatments may be highly beneficial or may require additional surface finish treatment or HIP treatment to obtain a higher fatigue strength improvement.

The main objective of this work is to analyze the effect of three surface treatments on the fatigue behavior of Ti6Al4V AM pieces manufactured by SLM. This effort includes an analysis of the surface roughness, the hardness profile close to the surface, the residual stresses and the defect distribution obtained with every treatment. The fracture surfaces after fatigue failure are analyzed to determine the crack initiation mechanisms associated with each failure, and the fatigue lives

obtained with the selected treatments are compared. SP and LP are the treatments selected for analysis. A third treatment consisting of shot peening followed by a surface treatment known as CASE and produced by Curtiss-Wright® was also considered. CASE is a type of chemically assisted tumbling, similar to the treatment known as extreme isotropic superfinishing (ISF®) [35,36] produced by REM®. This treatment reduces the roughness produced by shot peening, resulting in a piece with good surface finish and compressive residual stresses near it. A group of pieces that were sand blasted and annealed after manufacturing was analyzed as a reference for the surface-treated specimens. Sand blasting reduces the roughness, eliminating most of the unmelted particles adhering to the surface. Annealing reduces the anisotropy and eliminates the tensile residual stresses produced by the AM process. Considering the deleterious effect of the roughness, anisotropy and residual stresses of the as-built elements, before applying any surface treatment, all specimens were sand blasted and annealed.

This document is organized as follows. First, the materials and methods are described, indicating the manufacturing method and including the main parameters used, the surface treatments considered and their parameters, the procedures used to measure microhardness, surface roughness and residual stresses, and the test results. Next, the roughness and microhardness variation produced by each treatment are presented as well as the residual stress profiles and fatigue testing results. The fracture surfaces are also presented, showing the crack initiation points. The results are analyzed relating the crack initiation mechanisms with the treatments and the fatigue behavior. All of the results are discussed to understand the effect of the treatments. Finally, selected conclusions about the treatments are obtained.

2. Materials and methods

2.1. Specimens

The material of the specimens was Ti6Al4V, the chemical composition of which is given in Table 1. Twenty-four specimens were manufactured by SLM in a Renishaw AM250 SLM system with the following parameters: powder size, 15–45 μm; layer thickness, 60 μm; laser power output, 200 W; scan rate, 0.86 m/s; hatch distance, 95 μm; hatch rotation, 67°; argon gas atmosphere; and substrate heating to 150 °C. Additional details of the manufacturing parameters can be found in [56].

Because stress raisers are the typical fatigue crack initiation points and because most fatigue failures in real situations are initiated close to the surface at stress concentrations, a test procedure was designed to produce some type of stress gradient close to the specimen surface. Therefore, it was decided to use four-point bending to analyze the fatigue behavior. This type of test also reduces the uncertainties in stress produced during tests due to possible distortions produced by manufacturing. Fig. 1a depicts the geometry of the specimens. The test specimen sections were machined with corner radii of 2 mm, as shown in Fig. 1a, to avoid possible unintended defects in sharp corners. The largest dimension was oriented in the growth direction of the camera (z direction). This manufacturing direction was selected because it is usually the most unfavorable to resisting fatigue due to the adverse orientation of the main defects produced during manufacturing [10,57,58].

Before applying any other treatment or testing, all specimens were heat treated to eliminate residual stresses and sand blasted to clean the surface and reduce the roughness. The sand blasting parameters are shown in Table 2. The thermal treatment was annealing with the

following parameters: 730 °C for 2 h, slow cooling in the furnace, high-vacuum argon atmosphere.

2.2. Surface treatments

To compare the surface treatments, three different groups of six samples were selected. A different surface treatment was applied to the specimens of each group. For reference, a fourth group of six specimens was maintained without any additional treatment, except that sand blasting and annealing were applied to all of them. The treatments applied to every group were as follows:

Group 1: No surface treatment. This group serves as a reference and is referred to as "sandblasted" (SB). Two tests with SB specimens were invalid because of overloads produced during tests due to testing control system failures. Therefore, only four specimens were considered in this group.

Group 2: Shot peening was applied to all specimens in the group. The parameters of shot peening were as follows: 0.58 mm steel balls, 55–62 HRC ball hardness, 500% coverage and intensity 14A. This group is referred to as "shot peening" (SP).

Group 3: Two successive treatments were applied to this group. First, all specimens were shot peened with the same parameters as in Group 2. After shot peening, the specimens were subjected to CASE by Curtiss Wright®. CASE is a type of chemical-assisted vibration finishing. Samples are placed in a vibration-excited bowl containing an acid solution with a nonabrasive ceramic media. Next, the parts are reprocessed in a burnishing solution that restores the chemical stability and polishes the surface. As previously mentioned, this treatment is similar to the treatment known as extreme isotropic superfinishing (ISF®) [35,36] produced by REM®; it reduces the roughness produced by shot peening, resulting in a piece with good surface finish and compressive residual stresses near it. This group is referred to as "SP + CASE".

Group 4: The specimens were laser peened before testing. This treatment was carried out at the Department of Materials Science and Engineering, Saarland University, Germany. The treatment parameters were as follows: wavelength: 1064 nm; pulse length: 10 ns; round spot diameter: 2.6 mm; 6 repetitions of one-shot fields with 62% overlap; power density, 6 GW/cm^2. This group is referred to as "LP". Additional details of this treatment can be found in [56]. The used laser peening setup represents a low pulse energy laser with moderate beam quality and no given waveform control, which leaves room for further improvement of the process effects.

Considering that one face of the specimen will only be subjected to compressive stress during tests and that the depth of the compressive residual stress is 1.4 mm, only three faces of the specimen were treated to reduce the volume ratio of the peened to un-peened material. This will reduce the level of tensile stress in the un-peened zone.

2.3. Roughness measurement

Considering the paramount effect of roughness on fatigue strength [6,22,52], profile roughness was measured in all specimens of the four groups using a surface roughness profiler. The roughness was measured on the specimen surfaces where cracks initiated during the tests. The roughness was measured in the longitudinal direction of the test specimens (Z-direction according to Fig. 1a). It is expected that the surface roughness in the transverse direction (X-direction according to Fig. 1a) has a negligible effect on the fatigue behavior. The equipment used for linear roughness measurement was a Mitutoyo Surftest 501 instrument, with a probe tip radius of 5 μm. The evaluation length was 0.8 mm.

Table 1
Composition of the Ti6Al4V used for manufacturing the specimens.

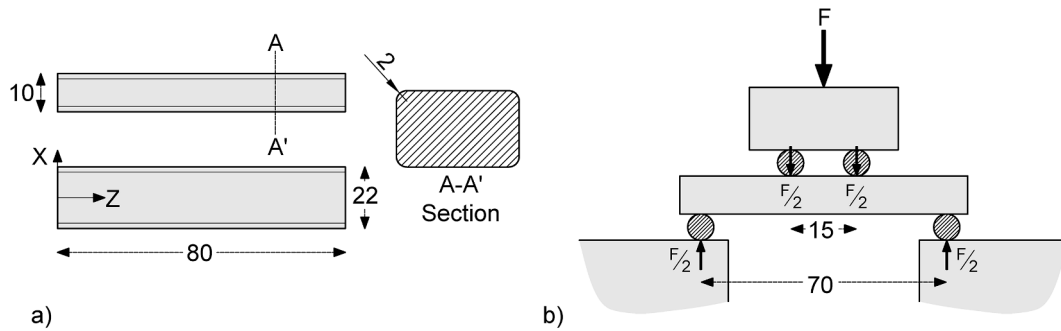| Element	Ti	Al	V	Fe	N	O	H	C
Composition/Weight%	Base material	5.5–6.76	3.5–4.5	<0.4	<0.03	<0.2	<0.015	<0.08

Fig. 1. a) Geometry of test specimens and b) scheme of the 4-point bending test setup. All dimensions are given in mm.

Table 2
Sand Blasting parameters.

Blasting material	Peening direction	Exposure time	Blasting pressure	Blasting distance
Glass microspheres	90° to the surface	15 s	5 bar	30 mm

Three measures were taken from each specimen. Therefore, 18 measures were obtained from groups 2 to 4, and 12 were obtained from group 1. Additionally, the area roughness was measured in one specimen for each treatment to obtain a better understanding of the surface topography. These measurements were carried out using a Sensofar S neox 3D optical profiler.

2.4. Micro-hardness measurements

Shot and laser peening produce microstructural transformations underneath the surface [59]. To determine whether those microstructural transformations have significant effects on the mechanical properties, a microhardness profile close to the surface was obtained for the three treatments. It was assumed that SP + CASE produces the same profile as SP alone. These microhardness profile measurements were carried out in a Phase II micro-Vickers hardness tester 900–390. The microhardness was measured up to a depth of 800 μm, with measurements taken at increments of 40 μm from the surface until 400 μm and increments of 100 μm from 400 to 800 μm, with the first measurement located at 20 μm from the surface. The load applied was 0.98 N. To avoid interferences between two contiguous indentations, for the first 400 μm, measurements were taken along inclined lines from the surface (22°) such that the distance between indentations for 40 μm of depth increments was at least 100 μm. Four inclined lines were selected, and four measurements were taken at each depth. Fig. 2 schematically depicts one of those lines used for microhardness measurement.

2.5. Metallurgical analysis

No change in the grain appearance was observed after LP. A characteristic dislocation structure, preferably close to the lath grain boundaries, could be seen. So the residual stress state can be reasonably assumed to be originated by the microstructural defect state. The SP specimens showed a gradient containing micro, ultra-fine grained and even nanocrystalline layer of α-phase close to the surface caused by heavy plastic deformation. A relatively sharp transition to the reference microstructure at depth of around 80 to 90 μm was observed. So, the residual stress state is assumed to be originated from both grain size and defect influences. A detailed metallurgical analysis can be found in another paper written by the authors and referred in the manuscript [56].
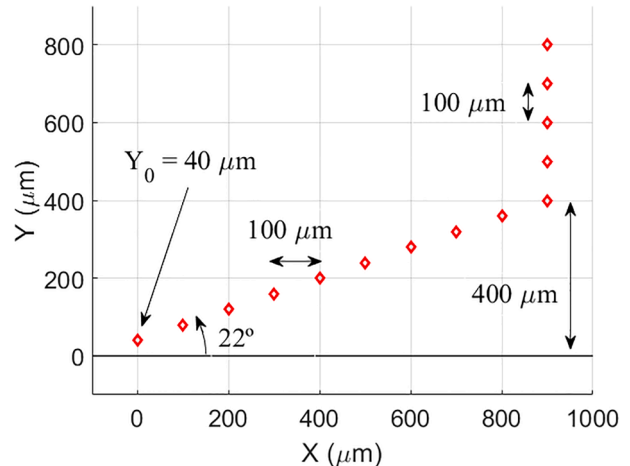
Fig. 2. Microhardness measurement along inclined lines to maintain a distance between indentations longer than 100 μm.

2.6. Residual stress measurements

Residual stress profiles close to the surface of the specimens for the four groups were measured by the blind hole drilling technique. A profile was obtained for each specimen of every group, and the mean and standard deviation of the measures at each depth were obtained for each group. The equipment used for drilling and measurement was the MTS3000 of SINT Technology®. The residual stress rosettes used were EA-031RE-120 from Vishay Micro-Measurement. The method used to calculate the stresses from the strain measurements was the Integral Method [60,61].

2.7. Fatigue tests

Fig. 1b shows the specimen and loading system for the four-point bending tests. Tests were carried out in an MTS 809 servo hydraulic push–pull testing machine. The test frequency was 8 Hz, and the stress ratio was R = 0.1. A sine waveform was applied and all tests were carried out in a controlled lab environment: 23 °C and 50% relative humidity. Tests finished with the final fracture of the specimen or after $5 \cdot 10^6$ without failure.

3. Results

3.1. Roughness

Fig. 3 depicts the roughness measurements (R_a and R_t) for the 4 groups in the longitudinal direction (Z-direction as shown in Fig. 1). In addition, Table 3 shows the average of the measures taken of the parameters R_a and R_t measured in the longitudinal direction and their
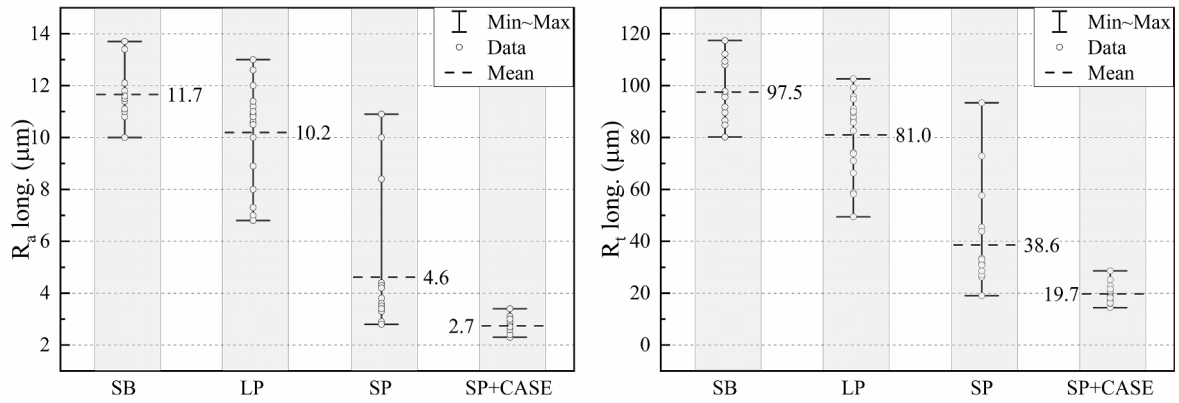
Fig. 3. Average roughness (R_a and R_t) for the 4 groups in the longitudinal direction (Z-direction).

Table 3

Average and standard deviation of surface roughness parameters (R_a and R_t) of specimen groups after treatments.

	SB	SP	SP + CASE	LP
R_a (µm)	11.7 ± 1.0	4.6 ± 2.4	2.7 ± 0.3	10.2 ± 1.9
R_t (µm)	97.5 ± 11.8	38.6 ± 18.6	19.7 ± 3.4	81.0 ± 15.3

standard deviation in each group.

The roughness produced after sand blasting is almost the same as that obtained by Bagehorn et al. [31]. after sand blasting and by Zhang et al. [62], who slightly sand-papered the as-built specimens to remove any lost powder from the surface. Very similar results were also obtained by Kahlin et al. [63], who also sand blasted the specimens after manufacturing. It can also be noted that LP produces almost no roughness reduction, and that SP reduces the roughness to less than 50%; a
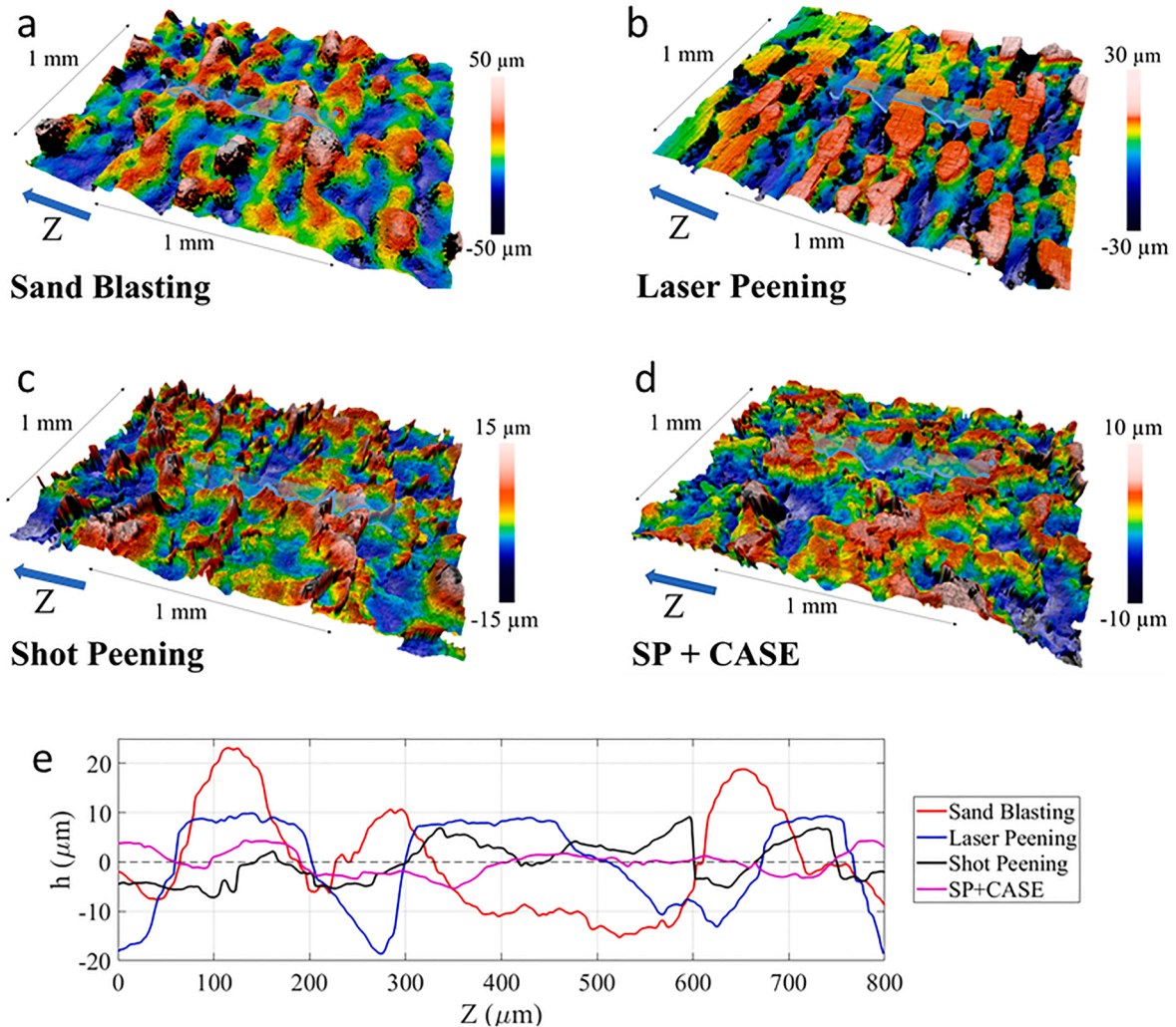

Fig. 4. 3D images of the surface roughness for the four surface treatments: a) SB; b) LP; c) SP and d) SP + CASE. e) Roughness profiles along the lines represented in a) to d).

similar result was also observed by Kahlin et al. [39]. Laser peening produces a plane shock wave on the spot area during each laser pulse. This pressure pulse applied to a rough surface generates slightly different multiaxial stress states following multiaxial strain states, depending on the topography, producing small differences of strains on the surface, which finally generates an almost uniform distribution of strain on the surface and thus very lightly changes the surface roughness. On the other hand, each ball impact during SP produces high compressive strains of the surface peaks and much lower pressures and strains on the troughs as well as higher pressures on the center of the impact zone than near the border of this zone. The result is a modification of the surface topography and, in the case of as-built specimens, a substantial roughness reduction. In the case of SP + CASE, the roughness reduction is higher; CASE divides by two SP roughness parameters, resulting in a total reduction to 25% of the initial roughness. Fig. 4 depicts 3D microscopic images of the surfaces of one specimen of each group. Fig. 4a to 4d show the surface roughness of SB, SP, SLP and SP + CASE, respectively. Fig. 4e shows the roughness profiles obtained along a line marked on the surface images, Fig. 3a to 3d. These figures show how the initial surface texture produced by SB is modified by the other three surface treatments. Additionally, Fig. 4e clearly shows the magnitude of the roughness reduction produced by each of the treatments relative to SB.

3.2. Hardness

Fig. 5 shows the hardness profiles from the treated surface to 0.8 mm in the specimens. A significant scatter of the measures was found at each depth. The differences between the maximum and minimum at each depth were close to 10–15 HV. Additionally, the difficulty of exactly fixing the depth of each measure produced some scatter of the depths for each theoretical measure. Considering this scatter, to determine the tendency, a moving average of the measures was obtained using 150 μm as the average interval. The scatter bands shown in the figure represent, for each treatment, the standard deviation between the four measurements obtained at each depth and the value represented by the curve. It can be observed in the figure that there is a very small variation in hardness among the three different surface treatments. For distances to the surface smaller than 400 μm, the SP specimen shows a small hardness increment, with the maximum value close to the surface, which is approximately 20 HV above the reference value. This increment is related to the microstructural changes produced by the treatment, as was observed by Slawik et al. [59] in samples with the same treatment parameters. In the LP specimens, the hardness increment close to the surface was smaller and almost negligible compared to the measuring scatter. This can be considered as a consequence of the small
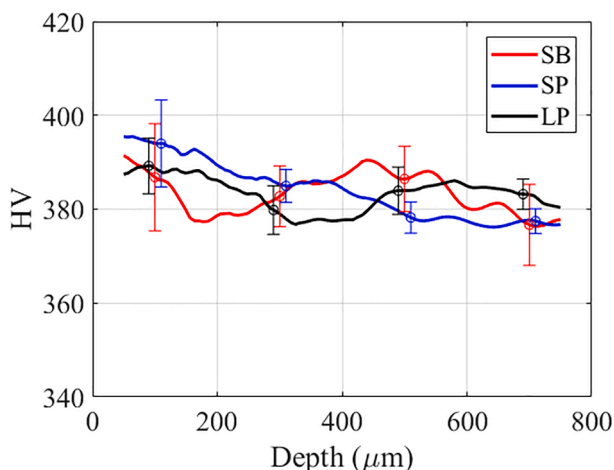
microstructural transformations close to the surface produced by this treatment. The third treatment considered, i.e., SB, did not produce any significant surface hardness variation relative to the bulk region. These results agree with the measurements made by Kahlin et al. [39], which did not detect significant variations in hardness close to the surface in specimens with the same treatments.

3.3. Residual stresses

Fig. 6 shows the in-depth residual axial stress profile [53]. The symbols represent the average value obtained for the six specimens of every group at different depths. The scatter bands of the six measurements at each point represent ± the standard deviation. It can be observed in the figure that the residual stress profiles obtained for SB, SP and LP via the blind hole method are similar to those obtained by X-ray diffraction [56]. The SB and SP residual stress profiles are similar to those obtained by Benedetti et al. [25]. Additionally, it is noteworthy that the maximum values of the compressive stresses produced by SP are higher than those produced by LP, but LP produces a deeper stress field; similar results have been found in [55] for cast materials. Moreover, as expected, the residual stress field produced by SB is confined to a region very close to the surface and with very low compressive stresses. On the other hand, it is remarkable to see how a surface treatment such as CASE can diminish the compressive residual stress below the surface produced by SP, although it can be considered small. Although these curves represent averages of six measures, part of this difference may also be a result of the scatter in the measures or of different surface finishes before adhering to the strain gauges.

4. Fatigue test results

Fig. 7 depicts the fatigue test results for 22 of the 24 specimens obtained in all tests [53]. As mentioned above, two tests with SB specimens were invalid because of overloads produced during tests due to testing control system failures. Each group of specimens is identified by a different symbol. The symbol is solid if the fatigue crack initiates from the interior of the sample or hollow if the fatigue crack initiates from the surface. It should be noted that although these results were shown in [53], some symbols changed from solid to hollow after a more detailed SEM analysis of the fracture surfaces. Some initial defects were assumed previously as internal defects were actually surface defects or internal defects with a connection to the surface. Lines fitting the results of each group are included.
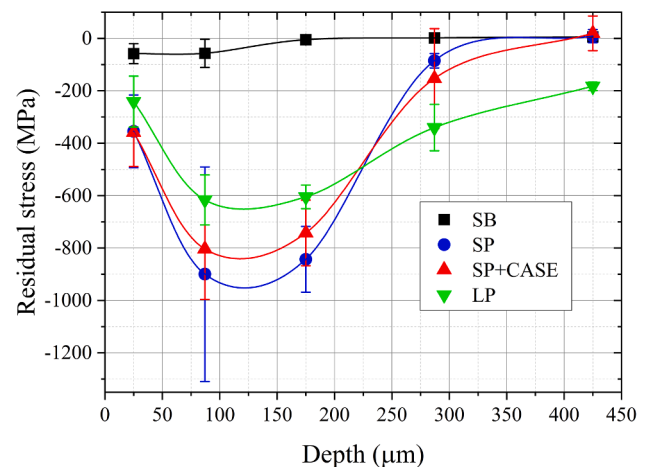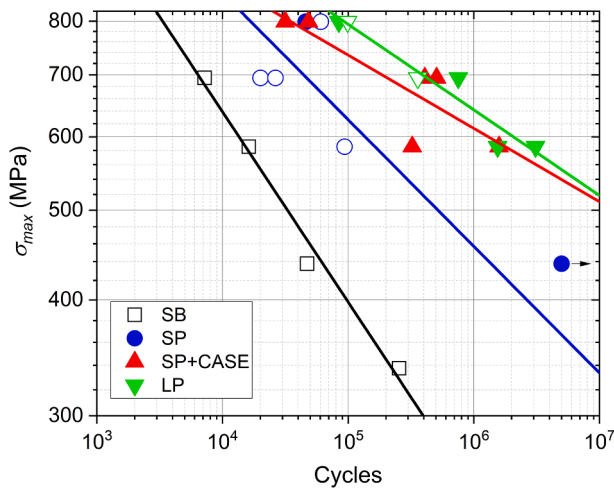

Fig. 5. In-depth hardness profile for different treatments.

Fig. 6. Residual stress produced by sand blasting, shot and laser peening, measured by the blind hole drilling technique [53].

Fig. 7. Fatigue test results ($R = 0.1$). Each group is identified with a different symbol. Symbols are shown as solid for failures initiated from the interior and hollow for failures initiated from the surface [53].

4.1. Fracture surfaces

Fig. 8 shows the fracture surface of four specimens, one from each group. Fig. 8a shows the initiation points on the surface of one SB specimen. It is easy to distinguish the defects where cracks were initiated, which are marked with arrows. Small white spots in the images are small pores produced during the manufacturing process. Fig. 8b, 8c and 8d depict the fracture surfaces of specimens treated with LP, SP and SP + CASE, respectively. It is worth noting that all SB specimens and three SP specimens failed with cracks initiated from defects on the surface, while only one LP specimen failed from surface defects, with all others failing with cracks initiated in the interior of the specimens. In the same way, all failures of SP + CASE specimens initiated in the interior.

Fig. 9a, 9b and 9c show SEM details of the initiation points, marked with arrows, of the fracture surfaces depicted in Fig. 8b, 8c and 8d, respectively. Fig. 9a represents the defect that initiated the crack in the LP specimen as well as three small pores close to the defect, marked with

smaller arrows. The same type of pores could be found on almost all fracture surfaces analyzed. Fig. 9b represents the lack of a fusion defect that initiated the crack in an SP specimen, while 8c shows an initiation point produced by a pore in an SP + CASE specimen.

By analyzing the fracture surfaces, different textures can be distinguished, depending on the distance to the initiation point (Fig. 8b). Close to the initial defect, the surface is shiny; as the distance to the initiation point increases, the surface becomes darker, and finally, the final failure surface becomes rougher and darker. The morphology of the surface in these zones can be observed in the SEM images shown in Fig. 10. As shown in Fig. 10a and 10b, due to the low plastic strains produced when the crack is small and grows with low ΔK, it is easy to see the α particles immersed in the matrix. Once the crack is longer and ΔK is higher, plastic strains are typical of long crack growth, far from the threshold, and striations, marked with arrows, can be observed (Fig. 10c). Finally, the final fracture zone presents the typical static fracture surface with many microvoids produced by plastic strain (Fig. 10d).

Regarding the position of the initiation points in specimens with different treatments, as aforementioned, in all SB specimens, the initial crack initiated on the surface, while most SP specimens and only two LP specimens failed from surface defects or internal defects connected to the surface; all other failures were generated by cracks initiated in the interior of the specimens. In the same way, all failures of SP + CASE specimens started with cracks initiated from interior defects. Fig. 11, which is a modification of the one shown in [53] and considering the SEM reanalysis of the initial defect position, depicts the position of all initiation points produced in the interior of the specimens for different treatments. All failures initiated at depths smaller than 2 mm.

Regarding the axial position, all failures were produced along sections situated axially between the upper rollers. In order to check that there was not a distortion of the stresses produced by the short distance between upper rollers a FE analysis of the stresses produced during tests was carried out. It was checked that there was a very small distortion in the stresses close to the tensile stressed face. Fig. 12 shows the axial position of sections where failures were produced, as well as the stress on the specimen surface relative to the theoretical stress produced along the specimen during the four point bending test. The axial position is measured from one of the top rollers and the stresses are represented
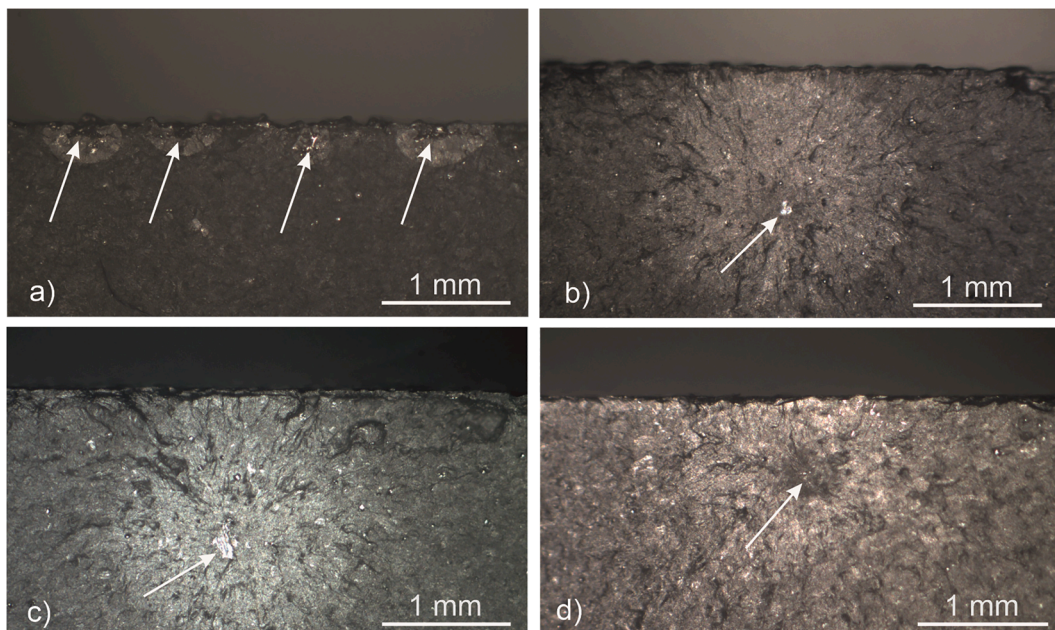
Fig. 8. Crack surfaces of specimens after failure. a) SB specimen, tested under S_{max} = 695 MPa (N_f = 7226 cycles); b) LP specimen, S_{max} = 799 MPa (N_f = 84,338 cycles); c) SP specimen, S_{max} = 799 MPa (N_f = 45,992 cycles); d) SP + CASE specimen, S_{max} = 585 MPa (N_f = 1,590,700 cycles).
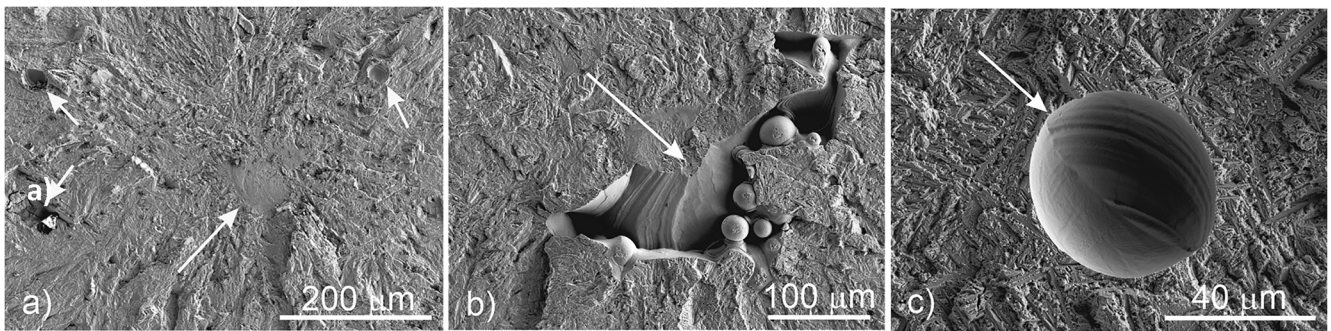
Fig. 9. SEM images of fracture surfaces with details of defects that initiated the cracks in specimens: a) LP, N_f = 84,338 cycles); b) SP, N_f = 45,992 cycles; and c) SP + CASE, N_f = 1,590,701 cycles.
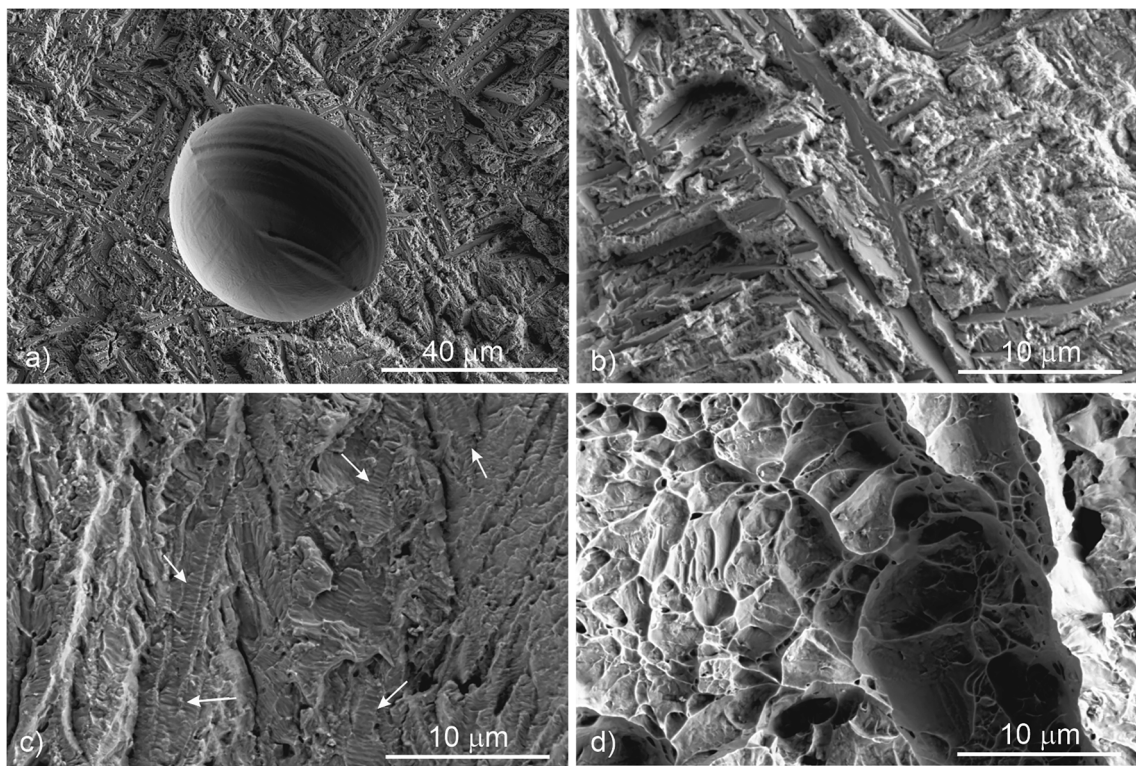

Fig. 10. Fracture surface of specimen: a) initiation point and short crack growth; b) transition from short to long crack growth; c) long crack growth zone (arrows show some striations zones); d) final fracture zone.
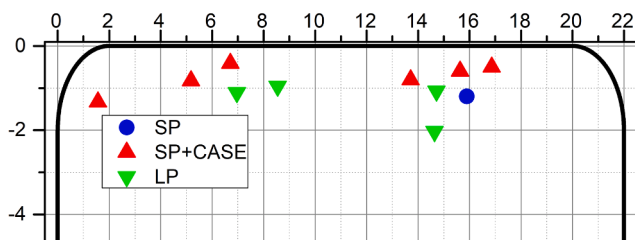

Fig. 11. Location of crack initiation in each test where the failure initiated from an interior defect. Scales are given in mm.

until half the distance between the top rollers since the stress distribution is symmetrical. It can be seen that the stresses at all surface points of the initiation sections ranged between 99% and 101% of the maximum theoretical stress.
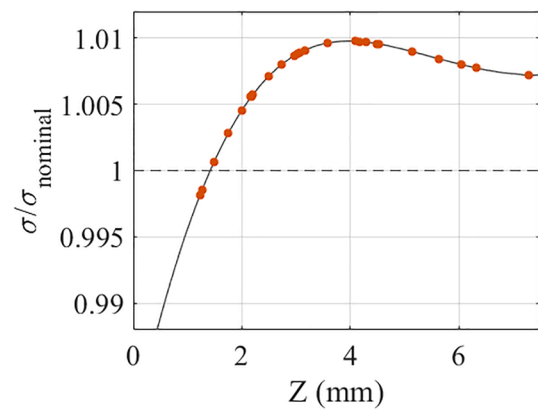

Fig. 12. Axial position of the crack initiation measured from one of the top rollers.

5. Discussion

The results of Fig. 7 show that the SB specimens are much less resistant than those treated with the other three treatments. In general, except in the case of a large internal defect close to the surface, as-built or SB specimens fail with cracks starting from a surface defect, so the behavior can be considered mainly dependent on the surface roughness and defects open to the surface. The fatigue lives of these specimens are located in the band shown by other researchers for materials that were only stress relieved or annealed after manufacturing the specimens or were stress relieved or annealed and SB applied [21,25,28,29,39,52,63–65], the effect of which on the as-built specimens is simply cleaning of the surface and a very small modification of the roughness. Fig. 13 shows the results obtained by those researchers compared with our results. The fatigue life is represented against the effective or equivalent stresses (σ_{eff}) associated with a stress ratio of R = 0, so that the results can be directly compared. The equation

$$\sigma_{eff} = \sigma_{max}(1 - R)^{0.29} \tag{1}$$

proposed by Walker and Dowling, [66–67], was used to transform the results obtained with other R values to the equivalent maximum stress with R = 0, where σ_{max} is the maximum stress in the tests, and σ_{eff} is the equivalent maximum stress for R = 0. The exponent in the equation should be fitted for each material and condition. In this case, a value of 0.29 was used for the exponent, according to experimental results obtained for unnotched conventionally fabricated Ti6Al4V annealed sheet specimens tested uniaxially with stress ratios ranging from R = -0.5 to R = 0.5, [68].

Our results are located in the central zone of the scatter band. It can also be noted that the scatter of all results is small for lives below 10^5 cycles but very large for longer lives, where the effect of the worst surface defect becomes very important, as usually occurs in any fatigue problem of pieces with defects.

The SP group shows a higher strength, with a strength increment of approximately 75% for high cycle fatigue and near 35% for approximately 10^4 cycles, as shown in Fig. 7. These results agree with those obtained by other researchers [25,39,52], as represented in Fig. 14, where a group of results found in the literature for Ti6Al4V is represented for comparison with our results. The residual stress field and the reduction in porosity near the surface, as demonstrated by Benedetti et al. [25], in conjunction with the improvement in the surface roughness generated by SP, produced a high increase in the fatigue strength.
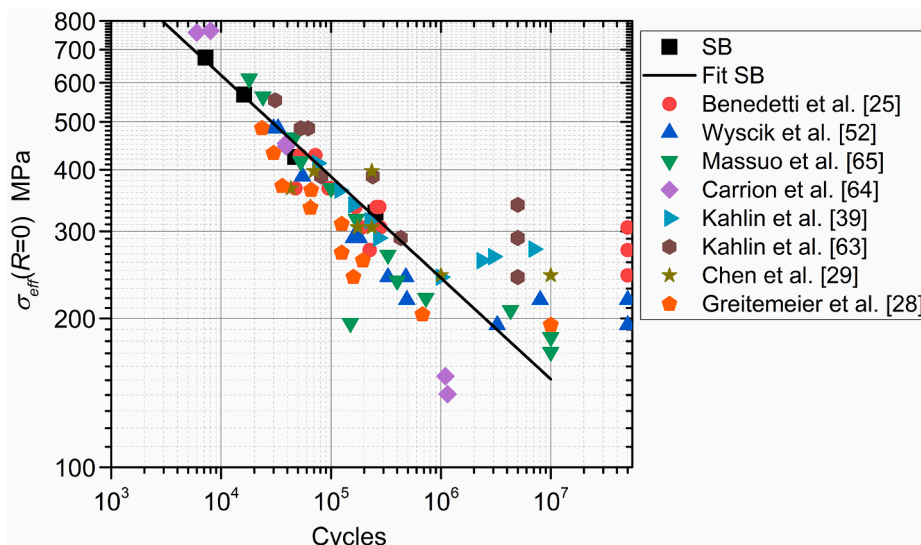

Fig. 14. Test results of SP specimens compared with other results in the literature for the same material.

Although in one specimen the failure initiated from an internal defect, all other specimens failed with cracks initiated from the surface. Although SP produces high local plastic strains, reducing the roughness and surface defects, some of these defects are transformed to microcracks, which can be the origin of fatigue failures [39]. Variations in the results from different researchers may depend on many parameters, especially on the initial defects of the specimens, the surface treatments applied before SP and the parameters used for manufacturing and SP.

Adding the CASE treatment to SP substantially improves the surface roughness and produces a very small variation in the residual stress field. The roughness is improved by eliminating the peaks of materials and with it some of the crack-like defects produced by the SP process. This reduces the probability of having failures starting from surface defects. Actually, in the tests carried out on these specimens, no failure was initiated from a surface defect. Fig. 7 shows that for $\sigma_{eff} = 640$ MPa, the stresses at which the SP and LP specimens failed from cracks initiated in the interior and lives were very similar. However, the tendency of the SP specimens to initiate cracks from crack-like defects on the surface for lower stresses opposite to SP + CASE specimens gives the SP + CASE specimens a higher fatigue strength. As a consequence of the CASE treatment, the fatigue lives increase relative to that of SP-only

Fig. 13. Fatigue test results for SB specimens compared to other results with the same material and similar stress relief and surface conditions in the literature.
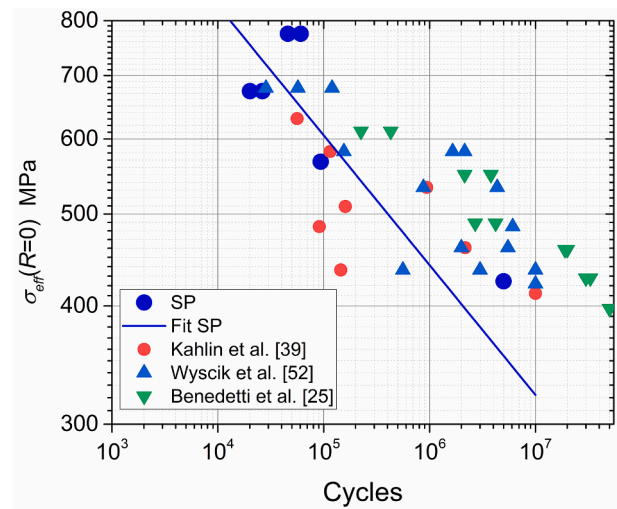
specimens by a factor close to ten for lives near 10^6 cycles (Fig. 7).

Finally, the group of specimens with LP treatment showed the best fatigue behavior among all treatments. The larger depth of the compressive residual stress field compared to the SP treatment, together with a very similar peak value, means that the cracks need higher cyclic stress values to develop until final failure, even considering that the surface roughness in this case is almost the same as that obtained for SB specimens. All specimens in this group failed with cracks initiated in the interior except for two. The high roughness of the LP specimens is the reason why two of the specimens in the group failed with cracks initiated from the surface or, as in one case, from an internal crack connected to the surface. Fig. 15 shows the test results obtained for SP + CASE and LP specimens and their tendency lines compared with results obtained by other researchers for LP [39] or HIP and machined, which is usually considered the treatment that produces the best results for Ti6Al4V AM specimens. The results obtained for LP are much better than those obtained with the same treatment and material by Kahlin et al. [39], probably because the residual compressive stress field produced by the LP treatment applied by Kahlin et al. was not as high as in our case, as noted in [39]. That group obtained peak values of the compressive stresses of −100 MPa, while in our case, the peak values are approximately −600 MPa. However, the residual stress field and fatigue strength improvement compared to the shot-peened specimens show the same tendency as those obtained by other researchers for AM specimens of different alloys [48] or for elements manufactured by traditional procedures [55]. It can also be observed that LP produces slightly better results than SP + CASE and that they are located in the band of some of the results produced for HIP and machined or polished specimens.

Regarding the position of the crack initiation points for the SP-, SP + CASE- and LP-treated specimens shown in Fig. 11, there are two effects that can be responsible for making the cracks initiate at a deeper location. One effect is the reduction of the defects close to the surface produced by SP, as shown by Benedetti et al. [25] for Ti6Al4V and other researchers for different alloys [38,69], and probably by LP, as shown by du Plessis et al. [54] for ALSi10Mg alloy, but not yet for Ti6Al4V, as far as authors know. An analysis of the possible reduction of defects close to the surface produced by SP and LP is a topic that authors plan to analyze in the near future. The other effect is the compressive residual stress field associated with each treatment. These residual stresses close to the surface cause the surface initial cracks to stop, allowing the growth of only cracks initiated below the residual stress field. The deeper compressive stress field and the probably higher depth of the porosity reduction produced by LP could explain the higher initiation depth

produced for that treatment.

To understand the effect of residual stress profiles, Fig. 16 shows the Smith-Watson-Topper (SWT) parameter variation with the depth during tests under load cycles for SP, SP + CASE and LP specimens. The points shown represent the initiation depth for each test and the value of the SWT parameter at that position for all specimens that failed from the interior. Note that the SWT parameter is normalized to the maximum in each test. Therefore, the normalized SWT parameter (SWT*) variation curve for each treatment has a very small variation from test to test, independent of the maximum stress applied in each case. According to this observation, for each treatment, all cases can be represented by a narrow band, as represented in the figure. This band is wider in the zone of residual stresses due to the normalization process. In this zone, the SWT parameter combines constant residual stresses with variable fatigue stresses. Therefore, the normalization of a constant value to variable maximum stresses, depending on the cyclic load applied, produces a different normalized value. The tendency to have an initiation defect near the zone where the maximum value of the damage parameter is produced can be observed. The large scatter of the initiation depth around the position of the maximum stress may be a result of the small stress gradients in the initiation zone, the defect position and size distribution and probably the tendency of SP and LP to reduce the size of the defects near the surface. Note that the SP and SP + CASE curves have been considered with the same residual stress profile for simplicity; in addition, they are represented by the same band.

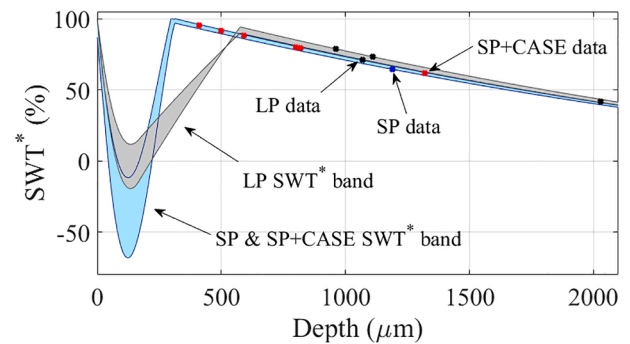Another way to analyze the position of crack initiation is through the

Fig. 16. Normalized SWT parameter (SWT*) evolution with depth for tests with SP, SP + CASE and LP specimens. Dots represent the initiation depth for different tests.
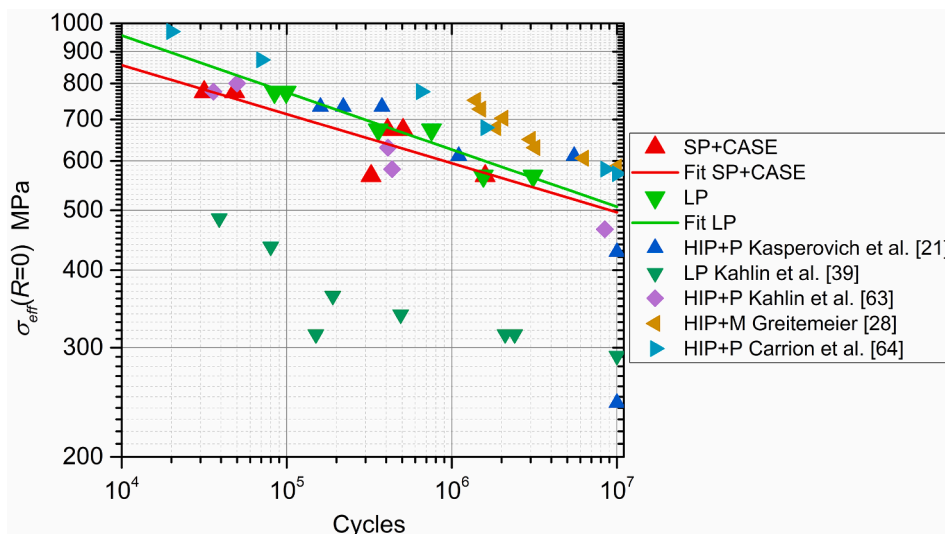

Fig. 15. Test results of SP + CASE and LP specimens compared with other results in the literature for the same material.

stress intensity factor. Considering that failures are initiated from a defect, the initial defect should be the combination of defect size and position producing the maximum stress intensity factor range (ΔK_I) so that it is higher than the fatigue crack growth threshold for that initial crack-like defect. Additionally considering the residual stress profiles produced by the treatments and attempting to obtain a first estimation of the zone for most likely crack initiation, Fig. 17 shows the ΔK_I values that could be produced by a hypothetical penny crack of 100 μm diameter as a function of its depth, also (as for SWT case) normalized to the maximum value in each test (ΔK^*). Only the positive part of K has been considered to estimate ΔK. To obtain a better understanding of the internal defect effect, each initiation point is marked with the initial defect size represented by the ratio between the square root of its area and that of the 100 μm penny crack. A tendency of small defects to initiate failure cracks only in the zone of the maximum stresses can be observed. They have to be the most detrimental defect in a zone of high stresses to produce a sufficiently high ΔK value. In contrast, larger defects may initiate failure cracks in the zone near the high ΔK value but also in deeper zones because they do not need such high stresses to produce a sufficiently high ΔK value.

Although this analysis gives some clues on the effect of different surface treatments on the fatigue behavior of AM Ti6Al4V pieces, a deeper analysis with a higher number of specimens for each treatment will allow getting a better understanding of the failure mechanisms associated to each treatment. This deeper analysis is planned by the authors to be done in the near future.

6. Conclusions

This paper addresses the effect that surface treatments such as SP, SP + CASE and LP have on the fatigue behavior of additive-manufactured Ti6Al4V specimens. The fatigue strength was studied using four-point bending tests. The fatigue behavior of only annealed and sand blasted specimens after AM is used as a reference. Selected conclusions can be obtained from the analysis:

The three treatments improved the fatigue strength.

The strength improvement is produced mainly via two effects: modification of the surface roughness and generation of a compressive residual stress field close to the surface.

SP reduces the surface roughness to approximately 50% of the original values and produces a tenfold increase in fatigue life relative to SB. One initiation point corresponds to a small defect in the interior of the specimen underneath the residual stress field generated by the treatment. However, the persistent high roughness and possible damage due to the treatment cause many tests to produce failure from a crack initiated on the surface.

SP + CASE produces an almost equal compressive stress field to SP but a smoother surface, improving the fatigue life relative to SP. The improvement of the surface roughness caused all the initiation points to be located in the interior of the specimen.

LP does not significantly modify the surface roughness and produces a residual stress distribution with a slightly lower peak but located deeper than that of SP, resulting in the highest fatigue strength of the three treatments analyzed. The high roughness of the specimens made two of them fail due to a crack initiated on the surface.

All failures initiated in the interior started from a defect located underneath the compressive residual stress field in the zone where the maximum stress intensity factor ranges were produced by the cyclic loads. This fact can be well represented by the SWT parameter variation along the specimen section or even better by a normalized ΔK value produced by a reference initial defect.

Other parameters that may influence fatigue behavior, such as the microstructure or possible reduction of pores produced by SP or LP, have not been studied at this point.
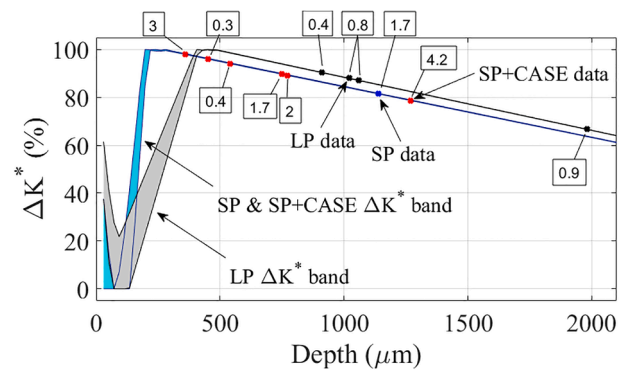

Fig. 17. Normalized ΔK parameter (ΔK^*) evolution with depth for tests with SP, SP + CASE and LP specimens. Dots represent the initiation depth for different tests.

Declaration of Competing Interest

The authors declare that they have no known competing financial interests or personal relationships that could have appeared to influence the work reported in this paper.

References

[1] Report W. 3D Printing and Additive Manufacturing. Wohlers Associates; 2019.
[2] Daniewicz SR, Shamsaei N. An Introduction to the fracture and Fatigue Behavior of Additive Manufactured Parts. Int J Fatigue 2017;94:167. https://doi.org/10.1016/j.ijfatigue.2016.07.007.
[3] Gorelik M. Additive Manufacturing in the Context of Structural Integrity. Int J Fatigue 2017;94:168–77. https://doi.org/10.1016/j.ijfatigue.2016.07.005.
[4] Chastand V, Quaegebeur P, Maia W, Charkaluk E. Comparative study of fatigue properties of Ti-6Al-4V specimens built by electron beam melting (EBM) and selective laser melting (SLM). Mater Charact 2018;143:76–81. https://doi.org/10.1016/j.matchar.2018.03.028.
[5] Tammas-Williams S, Withers PJ, Todd I, Prangnell PB. The influence of porosity on fatigue crack initiation in additively manufactured titanium components. Sci Rep 2017;7:7308. https://doi.org/10.1038/s41598-017-06504-5.
[6] Chan KS, Koike M, Mason RL, Okabe T. Fatigue life of titanium alloys fabricated by additive layer manufacturing techniques for dental implants. Metall. Mater. Trans. A Phys. Metall. Mater. Sci. 2013;44:1010–22. https://doi.org/10.1007/s11661-012-1470-4.
[7] Li P, Warner DH, Fatemi A, Phan N. Critical assessment of the fatigue performance of additively manufactured Ti–6Al–4V and perspective for future research. Int J Fatigue 2016;85:130–43. https://doi.org/10.1016/j.ijfatigue.2015.12.003.
[8] Galarraga H, Lados DA, Dehoff RR, Kirka MM, Nandwana P. Effects of the microstructure and porosity on properties of Ti-6Al-4VELI alloy fabricated by electron beam melting (EBM). Addit Manuf 2016;10:47–57. https://doi.org/10.1016/j.addma.2016.02.003.
[9] Nicoletto G. Anisotropic high cycle fatigue behavior of Ti–6Al–4V obtained by powder bed laser fusion. Int J Fatigue 2017;94:255–62. https://doi.org/10.1016/j.ijfatigue.2016.04.032.
[10] Yadollahi A, Shamsaei N. Additive manufacturing of fatigue resistant materials: Challenges and opportunities. Int J Fatigue 2017;98:14–31. https://doi.org/10.1016/j.ijfatigue.2017.01.001.
[11] Mercelis P, Kruth JP. Residual stresses in selective laser sintering and selective laser melting. Rapid Prototyping Journal 2006;12:254–65. https://doi.org/10.1108/13552540610707013.
[12] Fatemi A, Molaei R, Simsiriwong J, Sanaei N, Pegues J, Torries B, et al. Fatigue behaviour of additive manufactured materials: An overview of some recent experimental studies on Ti-6Al-4V considering various processing and loading direction effects. Fatigue Fract Eng Mater Struct. 2019;42:991–1009. https://doi.org/10.1111/ffe.13000.
[13] Chan KS. Characterization and analysis of surface notches on Ti-alloy plates fabricated by additive manufacturing techniques. Surf Topogr Metrol Prop 2013;3: 044006. https://doi.org/10.1088/2051-672X/3/4/044006.
[14] Li P, Warner DH, Pegues JW, Roach MD, Shamsaei N, Phan N. Towards predicting differences in fatigue performance of laser powder bed fused Ti-6Al-4V coupons from the same build. Int J Fatigue 2019;126:284–96. https://doi.org/10.1016/j.ijfatigue.2019.05.004.
[15] Gockel J, Sheridan L, Koerper B, Whip B. The influence of additive manufacturing processing parameters on surface roughness and fatigue life. Int J Fatigue 2019; 124:380–8. https://doi.org/10.1016/j.ijfatigue.2019.03.025.
[16] Pegues JW, Shao S, Shamsaei N, Sanaei N, Fatemi A, Warner DH, et al. Fatigue of additive manufactured Ti-6Al-4V, Part I: The effects of powder feedstock, manufacturing, and post-process conditions on the resulting microstructure and

defects. Int J Fatigue 2020;132:105358. https://doi.org/10.1016/j.ijfatigue.2019.105358.

[17] Gharbi M, Peyre P, Gorny C, Carin M, Morville S, Le Masson P, et al. Influence of various process conditions on surface finishes induced by the direct metal deposition laser technique on a Ti–6Al–4V alloy. J Mater Process Technol 2013;213:791–800. https://doi.org/10.1016/j.jmatprotec.2012.11.015.

[18] Günther J, Krewerth D, Lippmann T, Leuders S, Tröster T, Weidner A, et al. Fatigue life of additively manufactured Ti–6Al–4V in the very high cycle fatigue regime. Int J Fatigue 2017;94:236–45. https://doi.org/10.1016/j.ijfatigue.2016.05.018.

[19] Aboulkhair NT, Everitt NM, Ashcroft I, Tuck C. Reducing porosity in AlSi10Mg parts processed by selective laser melting. Addit Manuf 2014;1:77–86. https://doi.org/10.1016/j.addma.2014.08.001.

[20] Mancisidor AM, Garciandia F, Sebastian MS, Alvarez P, Diaz J, Unanue I. Reduction of the residual porosity in parts manufactured by selective laser melting using skywriting and high focus offset strategies. Phys. Procedia 2016;83:864–73. https://doi.org/10.1016/j.phpro.2016.08.090.

[21] Kasperovich G, Hausmann J. Improvement of fatigue resistance and ductility of TiAl6V4 processed by selective laser melting. J Mater Process Technol 2015;220:202–14. https://doi.org/10.1016/j.jmatprotec.2015.01.025.

[22] Yu H, Li F, Wang Z, Zeng X. Fatigue performances of selective laser melted Ti-6Al-4V alloy: Influence of surface finishing, hot isostatic pressing and heat treatments. Int J Fatigue 2019;120:175–83. https://doi.org/10.1016/j.ijfatigue.2018.11.019.

[23] Bagherifard CS, Beretta N, Monti S, Riccio M, Bandini M, Guagliano M. On the fatigue strength enhancement of additive manufactured AlSi10Mg parts by mechanical and thermal post-processing. Mater. Des. 2018;145:28–41. https://doi.org/10.1016/j.matdes.2018.02.055.

[24] Maawad E, Brokmeier HG, Wagner L, Sano Y, Genzel Ch. Investigation on the surface and near-surface characteristics of Ti–2.5Cu after various mechanical surface treatments. Surf. Coat. Technol. 2011;205:3644–50. https://doi.org/10.1016/j.surfcoat.2011.01.001.

[25] Benedetti M, Torresani E, Leoni M, Fontanari V, Bandini M, Pederzolli C, et al. The effect of post-sintering treatments on the fatigue and biological behavior of Ti-6Al-4V ELI parts made by selective laser melting. Journal of the Mech Behav of Biomed Mats. 2017;71:295–306. https://doi.org/10.1016/j.jmbbm.2017.03.024.

[26] Massuo H, Tanaka Y, Morokoshi S, Yagura H, Uchida T, Yamamoto Y, et al. Influence of Defects, surface roughness and HIP on the Fatigue Strength of Ti-6Al-4 Manufactured by Additive Manufacturing. Int J Fatigue 2018;117:163–79. https://doi.org/10.1016/j.ijfatigue.2018.07.020.

[27] Tammas-Williams S, Withers PJ, Todd I, Prangnell PB. The Effectiveness of Hot Isostatic Pressing for Closing Porosity in Titanium Parts Manufactured by Selective Electron Beam Melting. Metall Mater Trans A. 2016;47A:1939–46. https://doi.org/10.1007/s11661-016-3429-3.

[28] Greitemeier D, Palm F, Syassen F, Melz T. Fatigue Performance of Additive Manufactured TiAl6V4 Using Electron and Laser Beam Melting. Int J Fatigue 2017;94:211–7. https://doi.org/10.1016/j.ijfatigue.2016.05.001.

[29] Chen Z, Cao S, Wu X, Chris HJ, Davies CHJ. Surface roughness and fatigue properties of selective laser melted Ti6Al4V alloy. In: Froes FH, Boyer R, editors. Additive Manufacturing for the Aerospace Industry. Elsevier; 2019. p. 283–99. https://doi.org/10.1016/B978-0-12-814062-8.00015-7.

[30] Lee S, Pegues J, Shamsaei N. Fatigue Behavior and Modeling for Additive Manufactured 304L Stainless Steel: The effect of Surface Roughness. Int J Fatigue 2020;141:105856. https://doi.org/10.1016/j.ijfatigue.2020.105856.

[31] Bagehorn S, Wehr J, Maier HJ. Application of mechanical surface finishing processes for roughness reduction and fatigue improvement of additively manufactured Ti-6Al-4V parts. Int J Fatigue 2017;102:135–42. https://doi.org/10.1016/j.ijfatigue.2017.05.008.

[32] Pegues JW, Shamsaei N, Roach MD, Williamson RS. Fatigue life estimation of additive manufactured parts in the as-built surface condition. Mater. Des. Process. Commun. 2019;1:e36. https://doi.org/10.1002/mdp2.36.

[33] Kelly CN, Evans NT, Irvin CW, Chapman SC, Gall K, Safranski DL. The effect of surface topography and porosity on the tensile fatigue of 3Dprinted Ti-6Al-4V fabricated by selective laser melting. Mater Sci Eng, C 2019;98:726–36. https://doi.org/10.1016/j.msec.2019.01.024.

[34] Tyagia P, Goulet T, Riso C, Stephenson R, Chuenprateep N, Schlitzer J, et al. Reducing the roughness of internal surface of an additive manufacturing produced 316 steel component by chempolishing and electropolishing. Addit Manuf 2019;25 (32–38). https://doi.org/10.1016/j.addma.2018.11.001.

[35] Diaz A, McFadden P, Michaud N, Michaud J. Surface texture optimization of additive manufacturing metal components for improved mechanical performance. In ESIAM19, September 2019, Trondheim, Norway; 2019.

[36] Witkin DB, Patel DN, Helvajian H, Steffeney L, Diaz A. Surface Treatment of Powder-Bed Fusion Additive Manufactured Metals for Improved Fatigue Life. J Mater Eng Perform 2019;28:681–92. https://doi.org/10.1007/s11665-018-3732-9.

[37] Denti L, Bassolia E, Gatto A, Santecchia E, Mengucci P. Fatigue life and microstructure of additive manufactured Ti6Al4V after different finishing processes. Mater Sci Eng, A 2019;755:1–9. https://doi.org/10.1016/j.msea.2019.03.119.

[38] Lesyk DA, Martínez S, Mordyuk BN, Dzhemelinskyi VV, Lamikiz A, Prokopenko GI. Post-processing of the Inconel 718 alloy parts fabricated by selective laser melting: Effects of mechanical surface treatments on surface topography, porosity, hardness and residual stress. Surf Coat Technol 2020;381:125136. https://doi.org/10.1016/j.surfcoat.2019.125136.

[39] Kahlin M, Ansell H, Basu D, Kerwin A, Newton L, Smith B, et al. Improved fatigue strength of additively manufactured Ti6Al4V by surface post processing. Int J Fatigue 2020;134:105497. https://doi.org/10.1016/j.ijfatigue.2020.105497.

[40] Rosa B. Laser polishing of additive laser manufacturing surfaces. J Laser Appl 2015;27:S29102. https://doi.org/10.2351/1.4906385.

[41] Tian Y, Gora WS, Cabo AP, Parimi LL, Hand DP, Tammas-Williams S, et al. Material interactions in laser polishing powder bed additive manufactured Ti6Al4V components. Addit. Manuf. 2018;20:11–22. https://doi.org/10.1016/j.addma.2017.12.010.

[42] Lee S, Ahmadi Z, Pegues JW, Mahjouri-Samani M, Shamsaei N. Laser polishing for improving fatigue performance of additive manufactured Ti-6Al-4V parts. Opt Laser Technol 2021;134:106639. https://doi.org/10.1016/j.optlastec.2020.106639.

[43] Walker P, Malz S, Trudel E, Nosir S, ElSayed MSA, Kok L. Effects of Ultrasonic Impact Treatment on the Stress-Controlled Fatigue Performance of Additively Manufactured DMLS Ti-6Al-4V Alloy. Appl. Sci. 2019;9(4787). pp. 10.3390/app9224787.

[44] Zhang M, Liu C, Shi X, Chen X, Chen C, Zuo J, et al. Residual stress, defects and grain morphology of Ti-6Al-4V alloy produced by ultrasonic impact treatment assisted selective laser melting. Appl. Sci. 2016;6:304–11. https://doi.org/10.3390/app6110304.

[45] Sharp PK, Clayton JQ, Clark G. The fatigue resistance of peened 7050–T7451 aluminium alloy-repair and retreatment of a component surface. Fatigue Fract Eng Mater Struct 1994;17:243–52. https://doi.org/10.1111/j.1460-2695.1994.tb00226.x.

[46] Liu X, Liu J, Zuo Z, Zhang H. Effects of Shot Peening on Fretting Fatigue Crack Initiation Behavior. Materials 2019;12:743. https://doi.org/10.3390/ma12050743.

[47] Martín V, Vázquez J, Navarro C, Domínguez J. Effect of shot peening residual stresses and surface roughness on fretting fatigue strength of Al 7075–T651. Tribol Int 2020;142:106004. https://doi.org/10.1016/j.triboint.2019.106004.

[48] Hackel L, Rankin JR, Rubenchik A, King WE, Matthews M. Laser peening: a tool for additive manufacturing post-processing. Addit. Manuf. 2018;24:67–75. https://doi.org/10.1016/j.addma.2018.09.013.

[49] Uzan NE, Ramati S, Shneck R, Frage N, Yeheskel O. On the effect of shot-peening on fatigue resistance of AlSi10Mg specimens fabricated by additive manufacturing using selective laser melting (AM-SLM). Addit. Manuf. 2018;21:458–64. https://doi.org/10.1016/j.addma.2018.03.030.

[50] Bagherifard S, Berette N, Monti S, Riccio M, Bandini M, Guagliano M. On the fatigue strength enhancement of additive manufactured AlSi10Mg parts by mechanical and thermal post-processing. Mater Des 2018;145:28–41. https://doi.org/10.1016/j.matdes.2018.02.055.

[51] Maamoun AH, Elbestawi MA, Veldhuis SC. Influence of Shot Peening on AlSi10Mg Parts Fabricated by Additive Manufacturing. J. Manuf. Mater. Process 2018;2:40. https://doi.org/10.3390/jmmp2030040.

[52] Wycisk E, Emmelmann C, Siddique S, Walther F. High Cycle Fatigue (HCF) Performance of Ti-6Al-4V Alloy Processed by Selective Laser Melting. Advanced Materials Research 2013;816–817:134–9. https://doi.org/10.4028/www.scientific.net/AMR.816-817.134.

[53] Navarro C, Vázquez J, Domínguez J, Periñán A, Herrera-García M, Lasagni F, et al. Effect of surface treatment on the fatigue strength of additive manufactured Ti6Al4V alloy. Frattura ed Integrità Strutturale 2020;53:337–44. https://doi.org/10.3221/IGF-ESIS.53.26.

[54] du Plessis A, Glaser D, Moller H, Mathe N, Tshabalala L, Mfusi B, et al. Pore closure effect of laser shock peening of additively manufactured AlSi10Mg, 3D Print. Addit. Manuf. 2019;6:5. https://doi.org/10.1089/3dp.2019.0064.

[55] Vázquez J, Navarro C, Domínguez J. Experimental Results in Fretting Fatigue with Shot and Laser Peened Al 7075–T651 Specimens. Int J Fatigue 2012;40:143–53. https://doi.org/10.1016/j.ijfatigue.2011.12.014.

[56] Slawik S, Bernarding S, Lasagni F, Navarro C, Periñán A, Boby F, et al. Microstructural analysis of selective laser melted Ti6Al4V modified by laser peening and shot peening for enhanced fatigue characteristics. Mater Charact 2021;173:110935. https://doi.org/10.1016/j.matchar.2021.110935.

[57] Shamsaei N, Simsiriwong J. Fatigue Behaviour of Additively-Manufactured Metallic Parts. Procedia Struct Integrity 2017;7:3–10. https://doi.org/10.1016/j.prostr.2017.11.053.

[58] Molaei R, Fatemi A, Sanaei N, Pegues J, Shamsaei N, Shao S, et al. Fatigue of additive manufactured Ti-6Al-4V, Part II: The relationship between microstructure, material cyclic properties, and component performance. Int. J. Fatigue 2020;132:105363. https://doi.org/10.1016/j.ijfatigue.2019.105363.

[59] Lainé SJ, Knowles KM, Doorbar PJ, Cutts RD, Rugg D. Microstructural characterisation of metallic shot peened and laser shock peened Ti–6Al–4V. Acta Mater. 2017;123:350–61. https://doi.org/10.1016/j.actamat.2016.10.044.

[60] Schajer GS. Measurement of Non-Uniform Residual Stresses Using the Hole-Drilling Method. Part I—Stress Calculation Procedures. J Eng Mater Technol. 1988;110:338–43. https://doi.org/10.1115/1.3226059.

[61] Schajer GS. Measurement of Non-Uniform Residual Stresses Using the Hole-Drilling Method. Part II—Practical Application of the Integral Method. J Eng Mater Technol. 1988;110:344–9. https://doi.org/10.1115/1.3226060.

[62] Zhang J, Fatemi A. Surface roughness effect on multiaxial fatigue behavior of additive manufactured metals and its modelling. Theor Appl Fract Mech 2019;103:102260. https://doi.org/10.1016/j.tafmec.2019.102260.

[63] Kahlin M, Ansell H, Moverare JJ. Fatigue behaviour of notched additive manufactured Ti6Al4V with as-built surfaces. Int J Fatigue 2017;101:51–60. https://doi.org/10.1016/j.ijfatigue.2017.04.009.

[64] Carrion PE, Soltani-Tehrani A, Phan N, Shamsaei N. Powder Recycling Effects on the Tensile and Fatigue Behavior of Additively Manufactured Ti-6Al-4V Parts. JOM. 2019;71:963–73. https://doi.org/10.1007/s11837-018-3248-7.

[65] Massuo H, Tanaka Y, Morokoshi S, Yagura H, Uchida T, Yamamoto Y, et al. Effects of Defects, Surface Roughness and HIP on Fatigue Strength of Ti-6Al-4V manufactured by Additive Manufacturing. Procedia Struct Integrity 2017;7:19–26. https://doi.org/10.1016/j.prostr.2017.11.055.

[66] Walker K. The effect of stress ratio during crack propagation and fatigue for 2024–T3 and 7075–T6 aluminum. In: Rosenfeld M, editor. Effects Environment and Complex Load History on Fatigue Life. ASTM STP 462; 1970. p. 1–14. https://doi.org/10.1520/STP32032S.

[67] Dowling NE, Calhoun CA, Arcari A. Mean stress effects in stress-life fatigue and the Walker equation. Fatigue Fract. Eng. Mater. Struct. 2009;32:163–79. https://doi.org/10.1111/j.1460-2695.2008.01322.x.

[68] Metallic Materials Properties Development and Standardization (MMPDS-14), Chapter 5. Battelle Memorial Institute; 2019. http://app.knovel.com/hotlink/toc/id:kpMMPDSM11/metallic-materials-properties/metallic-materials-properties.

[69] Damon J, Dietrich S, Vollert F, Gibmeier J, Schulze V. Process dependent porosity and the influence of shot peening on porosity morphology regarding selective laser melted AlSi10Mg parts. Addit. Manuf. 2018;20:77–89. https://doi.org/10.1016/j.addma.2018.01.001.